City Research Online

City, University of London Institutional Repository

Behavior of oscillatory tube flow at liquid-gas interfaces

Katrin Bauer and Christoph Bruecker

Behavior of oscillatory tube flow at liquid-gas interfaces

Katrin Bauer and Christoph Bruecker
*Institute of Mechanics and Fluid Dynamics, TU-Bergakademie Freiberg, Akademiestr. 6,
09599 Freiberg, Germany*

Oscillatory flow in a long tube is characterized by an annular axial velocity profile far away from the boundaries for which an analytical solution exists. The radial velocity component is zero. Near the entrance or free surface region, this analytic solution does not hold due to the boundary conditions. Herein, the flow behavior at a liquid-gas as well as liquid-wall interface is investigated in detail by means of flow visualization measurements and Particle Image Velocimetry. The results suggest an additional radial velocity component due to the influence of the boundary. An investigation of the phase locked flow depicts the generation of steady streaming below the free surface which could be identified by vortex rings. Their shape and velocities vary according to the boundary conditions. For low frequencies, the streaming patterns are similar for cases with liquid-gas and liquid-wall interface denoting that the surface tension does not play a role for these cases. The oscillatory amplitude dominates streaming strength. As the Womersley number increases the free surface becomes unstable and Faraday waves occur which are further analysed here. This instability interacts with the steady streaming patterns which causes a change in shape and increases the streaming strength. © *2014 AIP Publishing LLC*. [http://dx.doi.org/10.1063/1.4890717]

I. INTRODUCTION

If a free surface is oscillated vertically instabilities evolve as a certain acceleration threshold is exceeded.[1] Above this threshold Faraday waves occur. Faraday[2] remarks that these waves have a frequency equal to one half that of the excitation. These free surface waves have been investigated for the capillary regime[1] as well as for the gravity-capillary regime.[3,4] Depending on the liquid viscosity and excitation frequency different surface patterns evolve.[3,5] Henderson and Miles[4] carried out stability analysis for Faraday waves both analytically as well as experimentally in small cylinders. Bronfort and Caps[6] found out that the threshold for instability increases as the liquid interface is covered by foam.

Considering the flow below the free surface another phenomenon can be observed which will be further addressed, here. The time average of oscillatory flow results in a non-zero mean flow known as steady streaming. A detailed survey about streaming effects and its mathematical treatment has been carried out by Riley.[7]

The occurrence of streaming in oscillatory flow is forced by Reynolds stress gradients which result in an additional body force term.[8,9] Since the body force terms are proportional to the Reynolds number it can be assumed that the streaming increases with increasing Reynolds number. Riley[10] introduced a modified Reynolds number $R_s = \epsilon^2 \cdot \alpha^2$ which denotes the magnitudes of mean convective effects to mean viscous effects. The dimensionless amplitude ϵ can be determined by $\epsilon = u_o/a \cdot \omega$. Here, u_o is the maximum driving velocity, a is the pipe radius, and ω the angular frequency. This definition is similar to the inverse of the Strouhal number. The variable α represents the Womersley number[11] which is a ratio of inertia to viscous forces in oscillatory flows with $\alpha = a\sqrt{\omega/\nu}$, ν is the kinematic viscosity. For very small Womersley numbers ($\alpha < 3$), quasi-steady flow can be assumed with velocity profiles similar to a laminar parabolic profile with the flow maximum in the pipe center. For increasing α, the velocity maximum is shifted towards the tube wall and the velocity profiles are characterized by an annular shape.

The effect of steady streaming is known in various applications such as oscillatory flows in tapered channels,[12] curved or flexible tubes.[13–15] In tubes with elastic walls such as arteries standing waves with total reflection lead to steady streaming effects comparable to those found in Kundt's dust tubes.[16] Yan[17] and Kotas et al.[18] observed streaming patterns around oscillating cylinders. More recently, Kumar et al.[19] designated steady streaming as a key mixing mechanism in the alveolar region of the human lung. Especially within micro-channels, steady streaming enhances mixing.[20,21] Oh et al.[22] found that steady streaming induced by oscillating micro-bubbles enhances drug delivery into tissue.

At large free surfaces travelling water waves generate an oscillatory motion which is responsible for steady streaming, here known as stokes drift.[23,24] The streaming causes mass transport of sediment as first described by Longuet-Higgins.[25]

In the case presented here, oscillatory flow in a vertical rigid tube with liquid-air interface at the top is studied. The length to diameter ratio of the tube is large. Hence, interference with the bottom boundary condition can be excluded. Far away from the top and bottom interfaces the flow is independent from the axial position in the tube and an analytical solution for the flow exists.[11,26] Near the free surface, the tangential stress at the interface induces steady streaming[9,27,28] which is investigated here in detail. The steady streaming patterns are analyzed by means of flow visualization as well as Particle Image Velocimetry (PIV) measurements under varying boundary conditions. The free surface break up conditions for varying frequencies and amplitudes are furthermore analyzed.

II. EXPERIMENTAL SETUP

Streaming is investigated in a vertically oscillating liquid column below the liquid-air interface at the top. The flow is generated within a transparent tube of 500 mm length (Fig. 1) and a diameter of $D = 12$ mm which is filled up to the height of $y = 400$ mm with two different oils (density $\rho = 840$ kg/m^3, kinematic viscosity $\nu = 31 \times 10^{-6}$ m^2/s (liquid 1), $\nu = 15 \times 10^{-6}$ m^2/s (liquid 2), surface tension $\sigma = 23$ mN/m). Harmonic oscillations of the fluid column in the tube are generated at the bottom via a piston connected to a magnetically driven shaker (VEB Messelektronik Otto Schoen, GDR). The oscillation amplitudes are about one order of magnitude smaller than the tube diameter. With the large length to diameter ratio the bottom wall disturbances do not influence the flow in the upper levels of the fluid column which has been proven by PIV measurements.
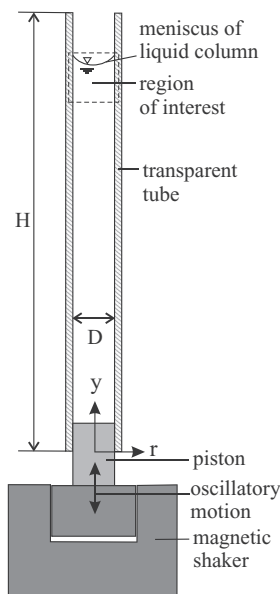

FIG. 1. Experimental setup (lengths ratios are not in true scale).

TABLE I. Experimental settings and values of the characteristic flow numbers at the interface of oscillatory tube flow.

Case no.	Frequency (Hz)	Amplitude (mm)	dim.less amplitude ϵ	Womersley number α Liquid 1	Womersley number α Liquid 2	Weber number We
1	5	0.5	0.08	6	8.7	0.05
2	10	0.5	0.08	8.5	12.3	0.22
3	15	0.5	0.08	10.5	15	0.5
4	20	0.5	0.08	12.1	17.4	0.9
5	25	0.5	0.08	13.5	19.4	1.3
6	30	0.5	0.08	14.8	21.3	1.9
7	10	0.7	0.12	8.5	12.3	0.4
8	10	1.0	0.17	8.5	12.3	0.9
9	10	1.25	0.21	8.5	12.3	1.3
10	10	1.5	0.25	8.5	12.3	1.9
11	10	1.75	0.3	8.5	12.3	2.6
12	15	0.83	0.14	10.5	15	1.3
13	20	0.63	0.1	12.1	17.4	1.3
14	30	0.42	0.07	14.8	21.3	1.3

The oscillatory flow behavior in the tube can be characterized by three different dimensionless numbers. These are the Weber number We, the Womersley number α, and a dimensionless amplitude ϵ as introduced above. The Weber number denotes the relation of fluid's inertia to surface tension with

$$We = \frac{\rho u^2 D}{2\sigma}. \tag{1}$$

Here, u is defined by the peak driving velocity with $u = A\omega$, where A denotes the excitation amplitude. The Capillary number Ca with $Ca = \nu\rho u/\sigma$ shall be further mentioned here as it denotes the relation of viscous forces to surface tension. Based on the maximum flow velocity a value of $Ca = 0.2$ is received. Hence, surface tension effects dominate the flow behavior near the interface in contrast to flows at $Ca \gg 1$ where viscous effects are important.[29] However, this number is not needed furthermore as its parameters are already considered by the above introduced dimensionless numbers. In addition, the Reynolds number is not used here, since the flow is dominated by surface tension effects and not viscous forces. Inertia is already considered by the Weber number.

The values of the relevant flow parameters set in the experiments are given in Table I. For these parameters steady streaming flow at the interface was investigated in detail. For flow characterization PIV measurements were carried out. Therefore, tracer particles (Fillite, hollow spheres) with a mean diameter of 20 μm were added to the liquid and the center plane of the pipe was illuminated by a 10 mJ Nd:YAG high speed laser (Pegasus, NewWave) with a wavelength of 532 nm. Images were recorded using a high speed camera (Photron, Fastcam PCI 1024). In order to visualize the steady streaming, phase locked images were taken. Therefore, a trigger signal was received from an accelerometer (KD 35, Metra Mess- und Frequenztechnik, Germany) connected to the oscillating element of the shaker. Hence, the image cross correlation was made between two subsequent periods at the same phase angle. The value of the phase angle is not important since steady streaming patterns do not depend on the phase angle. For all settings 100 images were taken and averaged in order to receive statistically firm results.

In order to analyze instabilities within the oscillatory tube flow, the maximum amplitudes and frequencies before the free surface becomes unstable were measured.

III. RESULTS

A. Mean flow near the stable interface

The mean motion of the fluid beneath the free surface is investigated, here. Fig. 2(a) exemplarily illustrates the typical streaming pattern at a frequency of 10 Hz and an amplitude of 1 mm.

This flow visualization (Fig. 2(a)) is received by superposition of 20 subsequent phase locked images. Vortical structures can be identified which form a toroidal vortex in the tube center if considered as axisymmetric flow and a smaller outer vortex ring near the wall. The streaming flow extends about one diameter into the pipe. Below, the influence of the free surface has vanished and the analytical solution for oscillatory pipe flow (see e.g. Uchida[26]) can be applied.

An image evaluation by cross correlation reveals the velocity vector plot (Fig. 2(b)). The velocity vector lengths indicate regions of higher and lower streaming velocity amplitudes. Maximum streaming velocity occurs in the tube center and is more than one order of magnitude lower than the maximum piston velocity. Both vortices are stretched in vertical direction, while the smaller vortex is further stretched in length up to three times of its diameter. The vortex pattern suggests the existence of a double boundary layer as described by Gaver and Grotberg[12] for a tapered channel.

The topology of the observed streaming pattern is illustrated schematically in Fig. 2(c). It is assumed that a similar pattern can be found in other oscillatory liquid flows with interfaces such as in liquid bridges (see e.g. Nicolas *et al.*[27]) or near end-walls.[9]

In order to prove that the flow far away from the boundaries is not influenced thereof, the velocity profile was measured in the middle of the tube by PIV and compared with the analytical solution. Fig. 3 shows a comparison of the analytical solution and experimental measurements for the case of 10 Hz and $A = 1$ mm. The experimental results are slightly off axis due to refractive index mismatch, however despite this deviation a good qualitative agreement of both profiles can be seen.

In the following each one of the characteristic parameters, as introduced above, is kept constant while varying the others in order to analyze steady streaming behavior.

1. Variation of the excitation amplitude at constant Womersley number

In this section, the results are presented for increasing amplitudes at constant frequency (Womersley number) and three different boundary conditions. Figs. 4(a) and 4(d) present results with a rigid wall as interface, Figs. 4(b) and 4(e) apply to the same liquid with free surface and for the cases shown in Figs. 4(c) and 4(f) the liquid viscosity was halved and with free surface again.

For all cases, the frequency was kept constant whereas the amplitude was linearly increased from $A = 0.5$ to 1.75 mm in 0.25 mm steps ($\epsilon = 0.08 - 0.3$). For cases of Figs. 4(a), 4(b), 4(d), and 4(e) the Womersley number is the same with $\alpha = 8.5$. For cases of Figs. 4(c) and 4(f), the Womersley number is increased to $\alpha = 12.3$ due to the lower viscosity.

In general, unbounded oscillatory pipe flows with constant Womersley number are characterized by an identical velocity profile and therefore the same stokes layer thickness.[26] As can be seen in
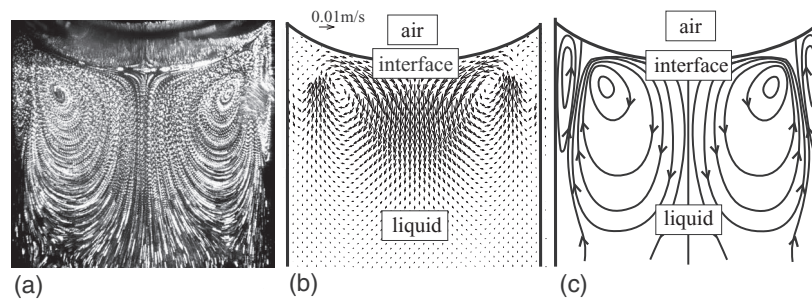

FIG. 2. Velocity vectors below the free surface for $f = 10$ Hz and $A = 1.00$ mm, (a) particle path images of the streaming motion as superposition of particle images for 20 subsequent periods, (b) velocity field obtained from cross-correlation, (c) typical vortex pattern (schematically).
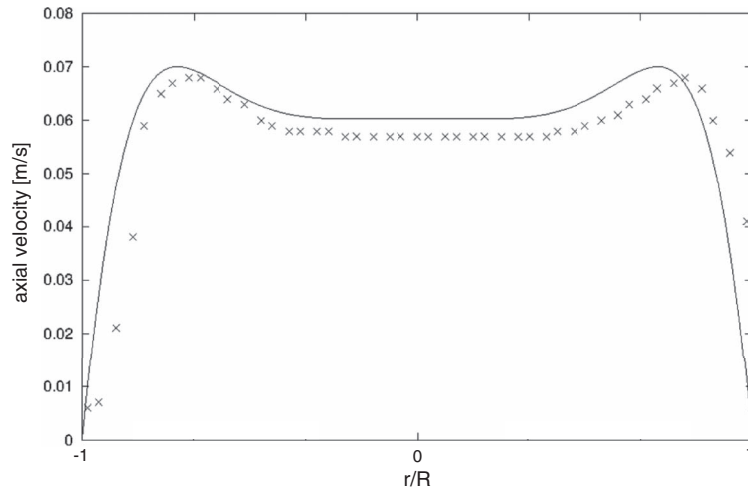
FIG. 3. Velocity profile in the tube far away from boundaries for $\alpha = 8.5$ and $\epsilon = 0.17$, $\times$ – experimental results, solid line – analytical solution.

Figs. 4(a)–4(f) the path lines of the particles suggest only small changes of the characteristic streaming patterns. This means despite those different boundary conditions, the streaming patterns are similar. The superposed particles presented in Figs. 4(a)–4(c) are shown as stripes whereas in Figs. 4(d)–4(f) single successive particles can be identified. This is due to higher streaming velocities which cause increased particle displacement within the same time-span.

Two counter rotating vortices can clearly be identified for the cases with free surface whereas the wall on top of the liquid obviously suppresses the second vortex. Consequently, the free surface curvature causes this second vortex. Nevertheless, it can also be seen that this smaller, second vortex has a smaller radial extension at decreased viscosity (compare Figs. 4(b) and 4(c)).
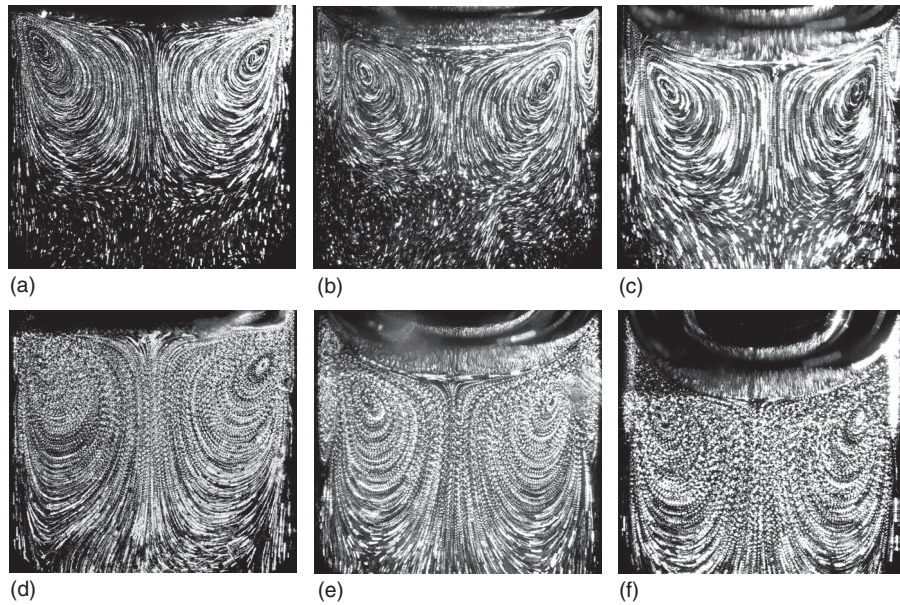
FIG. 4. Superposed particle images for 20 subsequent periods at $f = 10$ Hz, (a) liquid-wall interface, $\epsilon = 0.08$, $\alpha = 8.5$, (b) free surface, $\epsilon = 0.08$, $\alpha = 8.5$, (c) free surface, $\epsilon = 0.08$, lower viscosity ($\alpha = 12.3$), (d) liquid-wall interface, $\epsilon = 0.3$, $\alpha = 8.5$, (e) free surface, $\epsilon = 0.3$, $\alpha = 8.5$, (f) free surface, $\epsilon = 0.3$, lower viscosity ($\alpha = 12.3$).
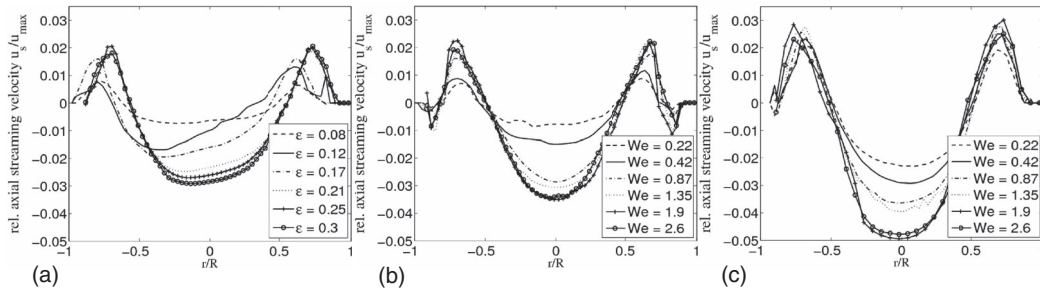
FIG. 5. Axial velocity profiles at the location of the maximum streaming velocity at $f = 10$ Hz for different amplitudes, (a) liquid-wall interface, $\alpha = 8.5$, (b) free surface, $\alpha = 8.5$, (c) free surface, $\alpha = 12.3$.

Increasing amplitudes lead to an increase of streaming penetration depth into the tube. For small amplitudes ($\epsilon = 0.08$, Figs. 4(a)–4(c)), the axial extension of the vortices is only about $0.5D$ below the free surface. As the amplitude increases up to $\epsilon = 0.3$ (Figs. 4(d)–4(f)) the axial extension of the inner vortex has almost doubled. The extension of the outer vortex (for the cases where it occurs), however, remained constant.

In order to quantify the streaming velocity u_s, the profiles of the axial velocity component at the axial position of the maximum streaming velocity are shown in Fig. 5. The streaming velocity is normalized with the maximum piston velocity u_{max}.

The maximum streaming velocity is observed at a dimensionless axial distance of $y/D = 0.3$ from the interface.

The Weber numbers are the same for the results presented in Figs. 5(b) and 5(c) as the surface tension did not change. Since the free surface is missing for the case presented in Fig. 5(a) the corresponding dimensionless amplitude is given in the figure legend.

The shape of the velocity profiles is similar for all amplitudes. However, it can be seen that for increasing amplitudes (Weber numbers) the dimensionless streaming velocity in the pipe center increases. This indicates a nonlinear dependency of the streaming velocity on the linear increasing amplitude.

A comparison of the velocity profiles reveals again the qualitatively similar streaming behavior for these three boundary conditions. For the case with wall interface, the peak velocity is slightly off axis. This is probably due to the slight gap between top wall and side wall of the tube. As can be identified in Fig. 4(a), a small second vortex developed at the top right corner, which cannot be found in the top left corner. The slight gap might have caused this vortex as well. Comparing experiments with the same liquid but with wall interface (Fig. 5(a)) and free surface (Fig. 5(b)) shows a peak velocity only 15% higher for the case with free surface. Whereas a comparison of liquids with high (Fig. 5(b)) and low viscosity (Fig. 5(c)) reveals an increase in peak velocity of 40%.

The results let us conclude that the surface tension and free surface curvature rather have a weak influence on steady streaming concerning both velocity magnitudes and pattern. In contrast, the liquid viscosity, i.e., the decreasing Womersley number and the excitation amplitude are the dominating factors which influence steady streaming, here.

2. Variation of the Womersley number α at constant amplitude

As presented above, increasing the oscillation amplitude at constant frequency leads to an increase of streaming pattern penetration depth and velocity. On the other hand, it is interesting to understand what happens at constant amplitude but increasing frequency (Womersley number).

Figs. 6(a)–6(c) show streaming patterns for liquid-wall interface at a constant excitation amplitude of $\epsilon = 0.08$ and increasing Womersley number. The same cases with free surface are presented in Figs. 6(d)–6(f). It is obvious that a constant amplitude causes similar streaming patterns for the cases with liquid wall interface. In contrast, the pattern shape changes strongly for increasing Womersley number for the cases with free surface (Figs. 6(d)–6(f)). From $\alpha = 6$ (Fig. 6(d)) to $\alpha = 10.5$ (Fig. 6(e)), the streaming pattern penetration depth has about doubled. Further increase of
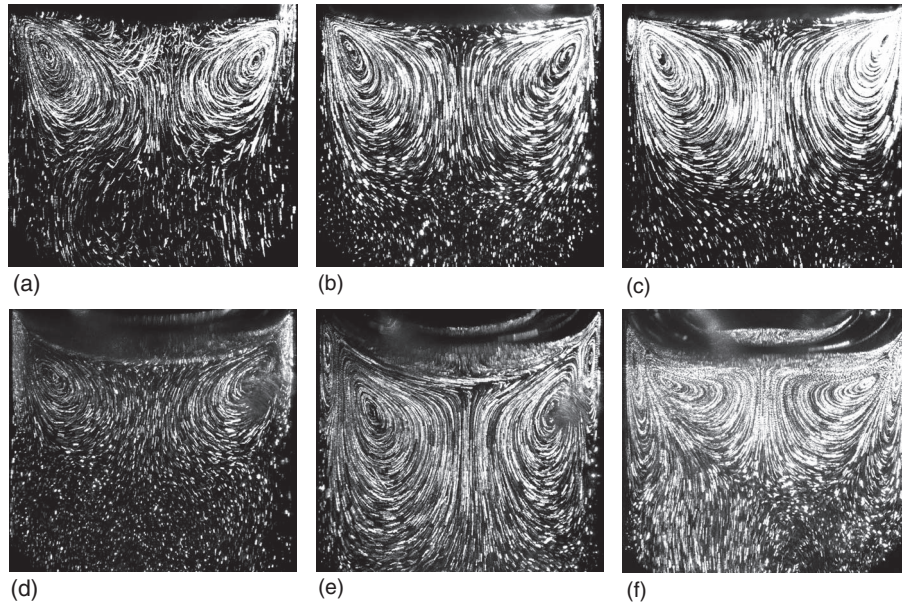
FIG. 6. Superposed particle images for 20 subsequent periods at $\epsilon = 0.08$ with liquid-wall interface (a)–(c) and free surface (d)–(f), (a) $\alpha = 6$, (b) $\alpha = 10.5$, (c) $\alpha = 14.8$, (d) $\alpha = 6$, (e) $\alpha = 10.5$, (f) $\alpha = 14.8$.

the Womersley number up to $\alpha = 14.8$ leads to a reversal of this effect and the axial extension of the streaming pattern decreases again. It needs further to be noticed that the free surface shape also changed from $\alpha = 10.5$ to $\alpha = 14.8$. At $\alpha = 14.8$ a convex deformation can be identified in the tube center. A closer look at the free surface motion within a period reveals that this convex deformation is not in phase with near wall free surface motion. While the near wall motion is already directed downwards the convex deformation still increases. This deformation on the axis of the tube changes during the upward motion of the liquid into a concave shape. Note that the excitation amplitude was always small enough so that the contact line of liquid at the wall did not move.

It is assumed that this free surface deformation denotes the initialization of the free surface instability. Experiments at even higher Womersley numbers (cf. Fig. 12) reveal a jet formation at the tube center which destructs the streaming patterns. This beginning instability strongly influences the streaming pattern.

The axial streaming velocity for the images presented above is depicted in Fig. 7. For the liquid-wall interface (Fig. 7(a)), the streaming velocity remains low at a similar level of about 0.5 mm/s. The free surface however causes a nonlinear increase of streaming velocity at increasing Womersley number up to three times of the values for liquid-wall interface.
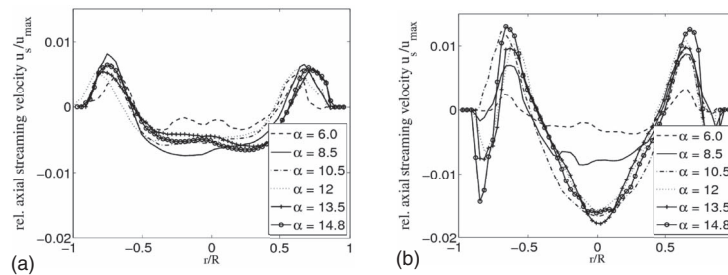

FIG. 7. Axial velocity profiles at the location of the maximum streaming velocity at $\epsilon = 0.08$ for liquid wall interface (a) and free surface (b) at different Womersley numbers.
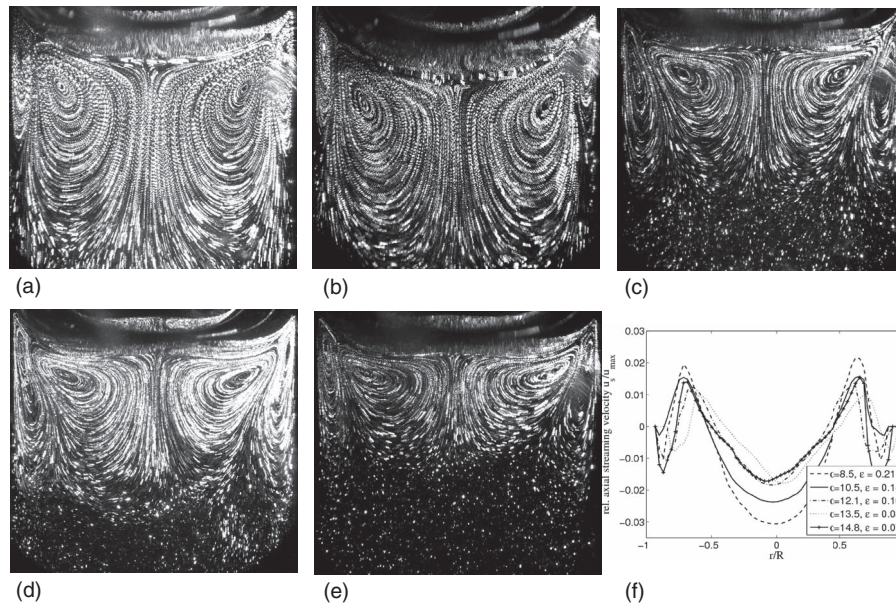
FIG. 8. Superposed particle images for 20 subsequent periods at We $= 1.3$, (a) $\alpha = 8.5$, $\epsilon = 0.21$, (b) $\alpha = 10.5$, $\epsilon = 0.14$, (c) $\alpha = 12$, $\epsilon = 0.10$, (d) $\alpha = 13.5$, $\epsilon = 0.08$, (e) $\alpha = 14.8$, $\epsilon = 0.07$, (f) profiles of axial velocity components.

3. Results for constant Weber number

In the following results are shown at constant Weber number of We $= 1.3$ but decreasing oscillating amplitude. This is achieved by increasing the Womersley number in the same amount as the amplitude decreases (see Table I). Note that, by doing this, the Reynolds number is kept constant as well. The results of the streaming patterns are presented in Fig. 8(a)–8(e) and the corresponding streaming velocities are depicted in Fig. 8(f).

It is obvious that both, streaming patterns and velocities differ strongly between the different cases. For lower Womersley numbers, the vortex is axially stretched (Figs. 8(a) and 8(b)). The cross sectional shape of the toroidal vortex resembles an oblate spheroid. As α increases the inner vortex changes into the shape of a triangle (Figs. 8(c)–8(e)). The radial extension of the outer vortex however increases. Consequently, the size of the inner and outer vortex is not related to the stokes layer thickness which decreases at higher Womersley numbers. The peak velocities decrease continuously from Fig. 8(a)–8(c) (cf. Fig. 8(f)) which is in accordance with decreasing amplitude which also leads to decreasing axial extension of the vortex pattern. A further decrease of amplitude (Fig. 8(d)–8(e) at increasing Womersley number does not change the axial streaming velocity, anymore (cf. Fig. 8(f)). For these cases the free surface is obviously dominated by the beginning instability in the tube center. This instability seems to compensate the influence of the decreasing amplitude. Hence, before an instability is initiated the steady streaming motion is strongly influenced by the excitation amplitude. The lower the amplitude the smaller are the streaming velocities and pattern extensions. The excitation velocities seem to be of minor importance as they were kept constant, here. The increasing Womersley number leads to instabilities.

B. Steady streaming according to Reynolds stress

As explained in the Introduction, the steady streaming motion is forced by Reynolds stress gradients. In this section, it will be proven that this also holds true for the investigated motion near the free surface. Therefore, PIV-measurements of the velocity vectors have been carried out. Altogether, 10 periods have been recorded with a resolution of 20 double-images per period. Exemplarily, the case of 10 Hz ($\alpha = 8.5$) and excitation amplitude of 0.5 mm ($\epsilon = 0.08$) has been chosen.
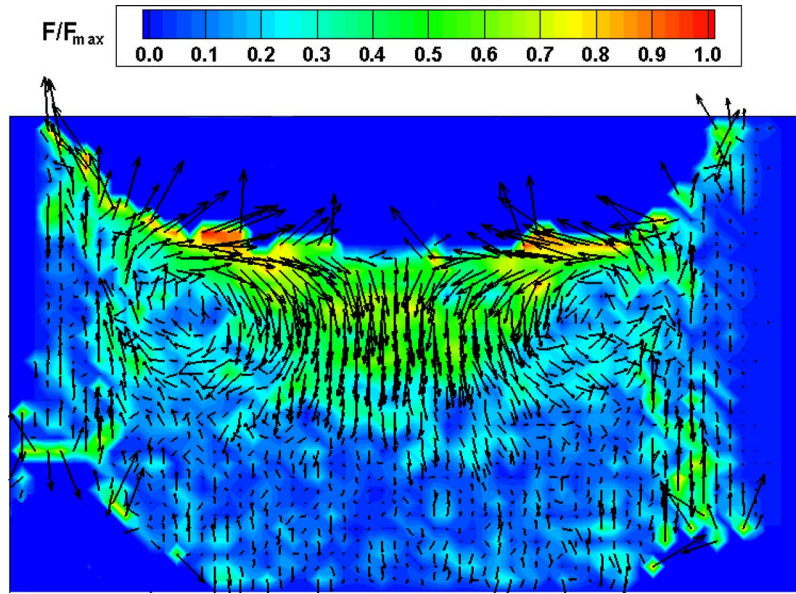
FIG. 9. Vector field of the Reynolds stress gradients at $\alpha = 8.5$ and $\epsilon = 0.08$, color contours represent the relative force magnitude F/F_{max}.

The spatial variation of the Reynolds stress which causes a net force leading to steady streaming can be calculated according to Lighthill[8]

$$F_j = \frac{-\partial(\overline{\rho u'_i u'_j})}{\partial x_i}.$$ (2)

The variable u'_i denotes the fluctuating velocity in the directions of x_i according to the Einstein notation ($i = 1, 2, 3$). F_j represents the net rate of change of x_j-momentum in the x_i direction.[8] Since, the PIV-data are only available in a plane, the force is calculated only in two directions according to

$$F_1 = -\rho \left(\frac{\partial(\overline{u'_1 u'_1})}{\partial x_1} + \frac{\partial(\overline{u'_2 u'_1})}{\partial x_2} \right),$$ (3)

$$F_2 = -\rho \left(\frac{\partial(\overline{u'_1 u'_2})}{\partial x_1} + \frac{\partial(\overline{u'_2 u'_2})}{\partial x_2} \right).$$ (4)

The differential equations (3) and (4) are discretized by a Central Differencing Scheme (CDS), since velocity data are only available on a discrete grid. The procedure is first to calculate an average velocity field from all data. Then determine the fluctuations u'_1 and u'_2 at each grid point and insert them into the discretized form of Eqs. (3) and (4). The resulting vector field F_j is illustrated in Fig. 9. The color contours represent the relative force magnitude.

Fig. 9 reveals a similar vortex structure as received directly by the phase locked measurements. This calculation has shown that a calculation of the Reynolds stress from phase locked velocity vectors yields the steady streaming structure.

C. Instability at the interface

The stability of the interface is influenced by pressure perturbations due to time-dependent fluid acceleration and capillary forces due to fluid-wall relative motion.[30] The resulting interface oscillations can be described by the Mathieu equation.[30,31] At excitation frequencies close to the natural frequency of the free surface wave, the surface becomes unstable and breaks up forming
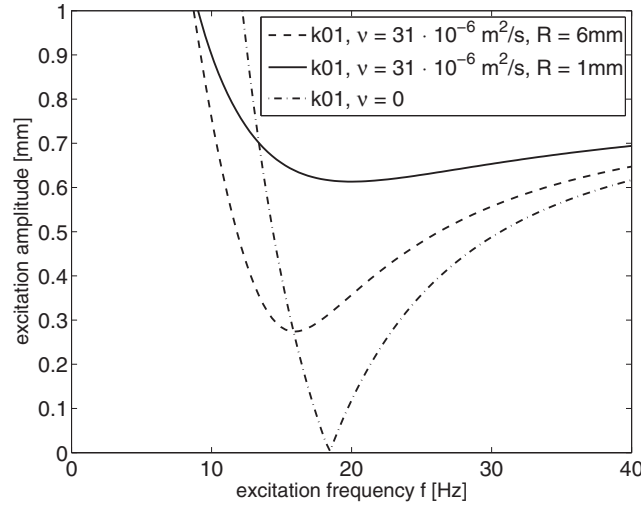
FIG. 10. Instability chart for the harmonic mode k_{01} for the conditions applied in the experiment (dashed line), smaller pipe radius (solid line), viscous free case (dashed-dotted line).

smaller droplets. The natural frequency can be calculated according to Royon-Lebeaud et al.[32]

$$\omega_{mn}^2 = g k_{mn} \left(1 + \frac{k_{mn}^2 \sigma}{g \rho} \right) \tanh(k_{mn} h). \tag{5}$$

Here, g denotes the gravity, h is the liquid depth, and k_{mn} is the wave number and the nth positive zero of the following equation:[4]

$$\left. \frac{d J_m(k_{mn} r)}{dr} \right|_{r=R} = 0. \tag{6}$$

$J_m(k_{mn} r)$ is a Bessel function of the mth order. If the term $g k_{mn}$ in Eq. (5) is smaller than $k_{mn}^3 \sigma / \rho$, the flow is dominated by capillary waves.[1] Here, both terms are similar. Hence, gravity-capillary waves are generated here and both terms have to be considered in Eq. (5).

The zeros of Eq. (6) give the axisymmetric and asymmetric modes, respectively. The results of Eq. (5) are valid only for the inviscid case. In order to incorporate damping by viscosity the parameter δ, denoting the ratio of actual to critical damping, is introduced according to Ref. 4. The natural frequencies are shifted to lower values due to the influence of viscosity. A new, viscous-shifted frequency $\hat{\omega}_{mn}$ can be calculated according to

$$\hat{\omega}_{mn} = \omega_{mn}(1 - \delta). \tag{7}$$

The forcing amplitude A_0 at which instability occurs is[4]

$$A_0 = [k_1 \tanh(k_1 h)]^{-1} \left[\delta^2 + \frac{(\omega^2 - \hat{\omega}_1^2)^2}{(2\omega^2)^2} \right]^{\frac{1}{2}}. \tag{8}$$

In Eq. (8), ω denotes the exciting angular frequency, k_1 and $\hat{\omega}_1$ are the wave number and viscous natural frequency of the $n = 1$ mode, respectively.

The stability chart for the harmonic mode k_{01} is shown in Fig. 10. The dashed-dotted curve denotes the case without damping, i.e., the inviscid case. The dashed curve represents the experimental conditions. Furthermore, a stability curve for a cylinder of smaller radius ($R = 1$ mm) is added.

As shown in Fig. 10, in case of no damping (dashed-dotted curve), i.e., viscosity is reduced to zero, the natural frequency is slightly shifted to higher values. However, the excitation amplitude to induce instability decreases to zero. Hence, the lower the viscosity of the liquid, the earlier instabilities set in. This behavior was also observed in the experiment. For the liquid with lower
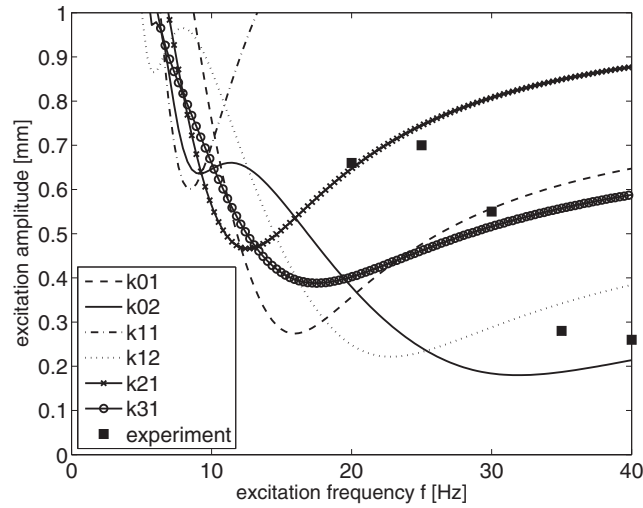
FIG. 11. Instability chart for several modes of *k*, experimental data are added by filled squares.

viscosity instability occurs at lower frequencies (at constant amplitude) and streaming velocities are higher. If the tube diameter is decreased (Fig. 10, solid curve), higher excitation amplitudes are necessary to induce instability.

In Fig. 11, the analytical results for several modes (symmetric and asymmetric) are presented based on the viscosity of the liquid which is used in the experiments. For frequencies below 10 Hz, instability occurs only at very high amplitudes. As the frequency increases, a minimum amplitude of about 0.2 mm at 30 Hz is necessary to induce a harmonic instability. As the amplitude further increases, single modes cannot be separated anymore. A superposition of harmonic and subharmonic oscillations will rather occur.

The points, at which instability of the free surface could be observed experimentally, were included for distinct frequencies in Fig. 11 (filled squares). The experimental values of the corresponding frequencies and amplitudes, at which instabilities were induced, are summarized in Table II.

The free surface behavior for beginning instabilities at frequencies from 20 Hz to 40 Hz is shown in Fig. 12.

For 20 Hz and 25 Hz (Figs. 12(a) and 12(b)), strongly asymmetric surface contours can be seen. It was further observed that these shapes oscillate with half of the excitation frequency which clearly indicates the characteristic of Faraday waves as described in the Introduction. Furthermore, as can be confirmed by the stability chart in Fig. 10(b), several harmonic and subharmonic modes are superposed, while the subharmonics dominate. The observed instability at 30 Hz (Fig. 12(c)) suggests harmonic behavior which can also be confirmed by the instability chart (Fig. 10(b)). Here, the value of 30 Hz is on the curve of the first harmonic mode (dashed line). At 35 and 40 Hz

TABLE II. Frequencies and amplitudes at which free surface instabilities start to occur.

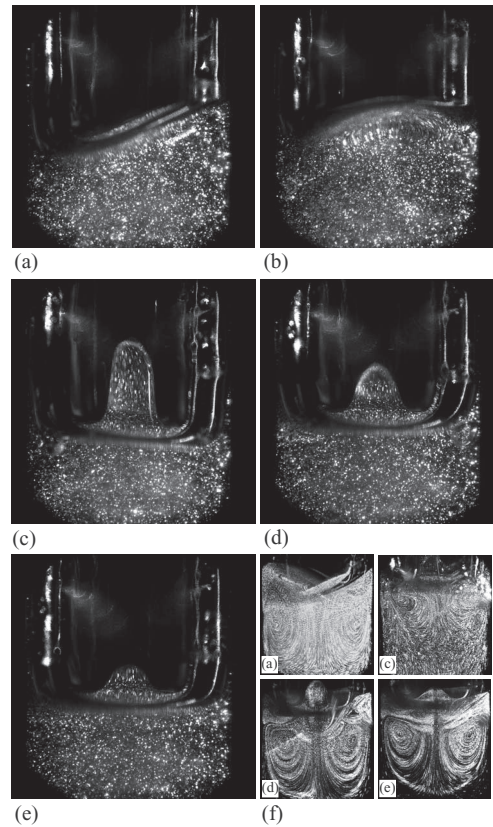| Frequency (Hz)	Amplitude A_0 (mm)
20	0.66
25	0.7
30	0.55
35	0.28
40	0.25

FIG. 12. Visualization of the free surface contour for varying frequencies of the piston at which harmonic and subharmonic instabilities occur, (a) 20 Hz, $A_0 = 0.66$ mm, (b) 25 Hz, $A_0 = 0.7$ mm, (c) 30 Hz, $A_0 = 0.55$ mm, (d) 35 Hz, $A_0 = 0.28$ mm, (e) 40 Hz, $A_0 = 0.25$ mm, (f) steady streaming patterns for cases (a), (c)–(e).

(Figs. 12(d) and 12(e)), the amplitudes to induce instability are strongly decreased and obviously, only the second harmonic mode (compare Fig. 10(b)) is existing.

Interestingly, despite the unstable interface, the steady streaming patterns still remain. These are shown exemplarily for Figures (a), (c), (d), and (e) in Fig. 12(f).

Other than in the theoretical results the experimental measurements did not suggest any instability below a frequency of 20 Hz. The maximum amplitude during the experiment was 1.75 mm at 1 Hz. An instability as the theoretical results suggest could not be observed. Generally, the instabilities occur at higher amplitudes as theoretically predicted. This behavior could be explained by two facts. First, the pipe radius is small so that capillary effects play a role and stabilize the surface waves. Second, the liquid column is large which means influences from the bottom can be neglected. Both facts do not apply to the experiments from Royon-Lebeaud et al.[32] and Henderson and Miles[4] from whose papers Eqs. (5)–(8) were deduced.

IV. CONCLUSION

In this study, the steady streaming and stability at the free surface of a vertically oscillating liquid column in a tube was analyzed. The Reynolds stresses caused by the interface boundary condition lead to a characteristic streaming pattern. It was found that at lower frequencies the influence of the free surface is negligible. By placing a light buoyant plate on the surface we could show that the streaming patterns as well as velocities were similar for the same liquid with and without free surface. An increase of amplitude, which is combined with an increase of velocity and Weber number causes a larger axial extension of the streaming pattern and consequently higher streaming velocities. It is argued that a variation in surface tension would lead to similar results. A change of the

viscosity only generates different streaming velocities, patterns are still similar. Larger frequencies, i.e., Womersley numbers lead to convex and concave free surface deformation. This deformation denotes the beginning of free surface instabilities that influence the near-surface streaming patterns. This effect is further enhanced by decreasing liquid viscosity.

It was furthermore found that the stokes layer thickness, governed by the Womersley number, is not related to steady streaming. Generally, the Womersley number only influences the shape of the streaming pattern.

ACKNOWLEDGMENTS

[1] K. D. Nguyem Thu Lam and H. Caps, "Effect of a capillary meniscus on the Faraday instability threshold," Eur. Phys. J. E **34**(10), 112 (2011).

[2] M. Faraday, "On a peculiar class of acoustical figures; and on certain forms assumed by groups of particles upon vibrating elastic surfaces," Philos. Trans. R. Soc. London **121**, 299–340 (1831).

[3] S. Douady, "Experimental study of the Faraday instability," J. Fluid Mech. **221**, 383–409 (1990).

[4] D. M. Henderson and J. W. Miles, "Single-mode Faraday waves in small cylinders," J. Fluid Mech. **213**, 95–109 (1990).

[5] A. Kudrolli and J. P. Gollub, "Patterns and spatiotemporal chaos in parametrically forced surface waves: A systematic survey at large aspect ratio," Physica D **97**(1–3), 133–154 (1996).

[6] A. Bronfort and H. Caps, "Faraday instability at foam-water interface," Phys. Rev. E **86**(6), 066313 (2012).

[7] N. Riley, "Steady streaming," Annu. Rev. Fluid Mech. **33**, 43–65 (2001).

[8] S. J. Lighthill, "Acoustic streaming," J. Sound Vib. **61**(3), 391–418 (1978).

[9] I. S. Goldberg, Z. Zhang, and M. Tran, "Steady streaming of fluid in the entrance region of a tube during oscillatory flow," Phys. Fluids **11**(10), 2957–2962 (1999).

[10] N. Riley, "Oscillating viscous flows," Mathematika **12**(2), 161–175 (1965).

[11] J. R. Womersley, "Method for the calculation of velocity, rate of flow and viscous drag in arteries when the pressure gradient is known," J. Physiol. (London) **127**(3), 553–563 (1955).

[12] D. P. Gaver and J. B. Grotberg, "Experimental investigation of oscillating flow in a tapered channel," J. Fluid Mech. **172**, 47–61 (1986).

[13] D. M. Eckmann and J. B. Grotberg, "Oscillatory flow and mass transport in a curved tube," J. Fluid Mech. **188**, 509–527 (1988).

[14] D. M. Wang and J. M. Tarbell, "Nonlinear-analysis of flow in an elastic tube (artery): Steady streaming effects," J. Fluid Mech. **239**, 341–358 (1992).

[15] C. A. Dragon and J. B. Grotberg, "Oscillatory flow and mass transport in a flexible tube," J. Fluid Mech. **231**, 135–155 (1991).

[16] R. B. Hastings and D. H. Ball, "Dust figures in a Kundt's tube," J. Acoust. Soc. Am. **7**, 59–63 (1935).

[17] B. Yan, "Oscillatory flow beneath a free surface," Fluid Dyn. Res. **22**, 1–23 (1998).

[18] C. W. Kotas, M. Yoda, and P. H. Rogers, "Visualization of steady streaming near oscillating spheroids," Exp. Fluids **42**(1), 111–121 (2006).

[19] H. Kumar, M. H. Tawhai, E. A. Hoffman, and C. Lin, "Steady streaming: A key mixing mechanism in low-Reynolds-number acinar flows," Phys. Fluids **23**(4), 041902 (2011).

[20] Z. Zhang, A. Fadl, C. Liu, D. M. L. Meyer, and M. Krafczyk, "Fluid streaming in micro/minibifurcating networks," J. Fluids Eng. **131**(8), 084501 (2009).

[21] G. Tanaka, M. Ohgawara, G. Inagaki, M. Hishida, and T. Sera, "Kinematic irreversibility of oscillatory flow in expanding and contracting small airways," Int. J. Heat Mass Transfer **55**(7–8), 1873–1880 (2012).

[22] J. S. Oh, Y. S. Kwon, K. H. Lee, W. Jeong, S. K. Chung, and K. Rhee, "Drug perfusion enhancement in tissue model by steady streaming induced by oscillating microbubbles," Comput. Biol. Med. **44**, 37–43 (2014).

[23] K. H. Kang and C. M. Lee, "Steady streaming of viscous surface layer in waves," J. Mar. Sci. Technol. **1**, 3–12 (1995).

[24] K. Gíslason, J. Fredsøe, R. Deigaard, and B. M. Sumer, "Flow under standing waves," Coastal Eng. **56**(3), 341–362 (2009).

[25] M. S. Longuet-Higgins, "Mass transport in water waves," Philos. Trans. R. Soc. London, Ser. A **245**(903), 535–581 (1953).

[26] S. Uchida, "The pulsating viscous flow superposed on the steady laminar motion of incompressible fluid in a circular pipe," ZAMP **7**, 403–422 (1956).

[27] J. A. Nicolás, D. Rivas, and J. M. Vega, "On the steady streaming flow due to high-frequency vibration in nearly in viscid liquid bridges," J. Fluid Mech. **354**, 147–174 (1998).

[28] C. P. Lee, A. V. Anilkumar, and T. G. Wang, "Streaming generated in a liquid bridge due to nonlinear oscillations driven by the vibration of an endwall," Phys. Fluids **8**(12), 3234–3246 (1996).

[29] D. P. Gaver III, O. E. Jensen, and D. Halpern, "Surfactant and airway liquid flows," Lung Surfact. Funct. Disorder **201**, 191–227 (2005).

[30] T. Ito, Y. Tsuji, and Y. Kukita, "Interface waves excited by vertical vibration of stratified fluids in a circular cylinder," J. Nucl. Sci. Technol. **36**(6), 508–521 (1999).

[31] C. R. Tipton and T. Mullin, "An experimental study of Faraday waves formed on the interface between two immiscible liquids," Phys. Fluids **16**(7), 2336–2341 (2004).

[32] A. Royon-Lebeaud, E. J. Hopfinger, and A. Cartellier, "Liquid sloshing and wave breaking in circular and square-base cylindrical containers," J. Fluid Mech. **577**, 467–494 (2007).